Published in final edited form as:
J Biomech Eng. 2010 November ; 132(11): 111005. doi:10.1115/1.4002491.

The Effect of Implantation Orientation of a Bileaflet Mechanical Heart Valve on Kinematics and Hemodynamics in an Anatomic Aorta

Iman Borazjani and **Fotis Sotiropoulos**
St. Anthony Falls Laboratory, University of Minnesota, Minneapolis, MN 55414

Iman Borazjani: iman@buffalo.edu; Fotis Sotiropoulos: fotis@umn.edu

Abstract

We carry out three-dimensional high-resolution numerical simulations of a bileaflet mechanical heart valve under physiologic pulsatile flow conditions implanted at different orientations in an anatomic aorta obtained from magnetic resonance imaging (MRI) of a volunteer. We use the extensively validated for heart valve flow curvilinear-immersed boundary (CURVIB) fluid-structure interaction (FSI) solver in which the empty aorta is discretized with a curvilinear, aorta-conforming grid while the valve is handled as an immersed boundary. The motion of the valve leaflets are calculated through a strongly coupled FSI algorithm implemented in conjunction with the Aitken convergence acceleration technique. We perform simulations for three valve orientations, which differ from each other by 45 deg and compare the results in terms of leaflet motion and flow field. We show that the valve implanted symmetrically relative to the symmetry plane of the ascending aorta curvature exhibits the smallest overall asymmetry in the motion of its two leaflets and lowest rebound during closure. Consequently, we hypothesize that this orientation is beneficial to reduce the chance of intermittent regurgitation. Furthermore, we find that the valve orientation does not significantly affect the shear stress distribution in the aortic lumen, which is in agreement with previous studies.

1 Introduction

Patients with heart valve disease commonly undergo surgery to replace their diseased valves with artificial ones. More than half of all the replaced valves are mechanical heart valves (MHVs), which unlike bioprosthetic valves have outstanding durability due to their material properties (see Fig. 1(*a*)), for a typical bileafelt MHV (BMHV). However, currently all MHV designs are strongly thrombogenic and the recipients are required to consume anticoagulation drugs for the rest of their lives. The exact mechanism of thromboembolism in MHVs is not fully understood, yet the hemodynamic factors such as shear stress [1,2], flow separation, and turbulence [3,4] are widely believed to be linked with thrombus formation. Therefore, a large number of studies have extensively researched the MHV-induced hemodynamics both experimentally [5–12] and computationally [13–21]. For a detailed assessment of the experimental and computational state-of-the-art in MHV flows, the reader is referred to the review papers in Refs. [22,23].

An important issue that has received considerably less attention in previous work is the impact of valve implantation orientation on valve performance in anatomic patient-specific geometries. Previous work has indicated that both valve type and implantation orientation affect the valve performance in terms of turbulent Reynolds stresses and pressure drop across the valve in an in vitro model [24]. In an animal study [25], different orientations of a MedTronic Hall tilting-disk MHV(TMHV) and a St. Jude BMHV were compared in terms of maximum Reynolds stresses normally occur during peak systole. It was found that the

Reynolds stresses in the downstream of the TMHV were almost similar to the native physiological valve when its major orifice was facing the right posterior wall, i.e., the region of the noncoronary cusp (NCC) [25]. The BMHV Reynolds stresses were higher than the native physiologic valve but did not change much for different valve orientations [25]. The best result for the BMHV in terms of Reynolds stresses was found when one orifice was oriented toward the right cusp, i.e., the area of the major flow was distributed equally among the two side orifices and the central slit [25]. Such good systolic performance (in terms of Reynolds stresses) was attributed to the asymmetric velocity profile, with highest velocities along the noncoronary cusp, at the inflow of the aortic valve due to the angle between the longitudinal axes of the left ventricle and the aortic root [26] (see Fig. 1(*b*)) for the related anatomy. Following this animal study, the systolic performance of both TMHV and BMHV designs was investigated in clinical studies [26–28]. The TMHV showed superior performance in terms of downstream turbulent Reynolds stresses relative to the BMHV, especially for smaller valve sizes [26]. The effect of valve orientation on diastolic performance has yet to be investigated in such detail [28]. Nevertheless, some work aimed at assessing the effects of valve orientation for both BMHV and TMHV in an animal model (pigs) by measuring the coronary flow rate [29]. This work showed that the coronary flow was significantly influenced by the valve orientation and for both TMHV and BMHV, the previous systolic optimum orientations in terms of Reynolds stresses [25] demonstrated higher left anterior descending flow rates [29]. More recently, the effect of valve orientation on coronary perfusion pressure has been investigated [30]. It was found that the differences in myocardial perfusion pressure between different orientations of a BMHV or between BMHV prostheses and bioprostheses are small and essentially negligible [30].

It follows from the above literature review that all previous studies on the effect of MHV implantation orientation on valve performance have gauged performance in terms of Reynolds stresses for systolic performance and coronary flow rate and pressure for diastolic performance. The effect of orientation on the ensuing valve kinematics, the amount of leakage flow, and viscous shear stress are topics that to date remain entirely unexplored. Furthermore, and as discussed by Ge et al. [31], the Reynolds stresses are not physical forces but rather a statistical quantity that cannot induce actual force since the size of the Kolmogorov scale (i.e., the size of the smallest vortices in a turbulent flow) in physiologic MHV flows is much larger than the blood cell size. This suggests a need for a paradigm shift in MHV research from measuring the turbulent statistics to experimental and numerical methods that can quantify the instantaneous viscous forces. In our previous work, we developed and validated a fluid-structure interaction (FSI) solver that can simulate the flow and motion of a BMHV implanted in an axisymmetric aorta to accurately quantify the instantaneous viscous forces at physiologic conditions [32]. The simulated results were in excellent agreement with in vitro experiments [5] and could capture all flow features [32]. More recently, we applied the FSI solver to simulate the flow through a BMHV implanted in an anatomical aorta and compared the valve kinematics and hemodynamics with those obtained from the straight axisymmetric aorta computations [33]. We showed that the aorta geometry has a significant effect both on the valve motion and hemodynamics [33]. Such image-guided simulations constitute the first step toward the goal of patient-specific MHV implantation surgical planning, during which different implantation orientations and different valves can be compared and an optimal valve design and implantation orientation can be identified before surgery.

In this paper, we take a step further toward patient-specific valve implantation surgical planning by carrying out high-resolution FSI numerical simulations to investigate the effect of BMHV implantation orientation in an anatomic aorta and at physiologic conditions. We employ the same aorta geometry, BMHV design, and inflow wave form used by Borazjani et al. [33] and carry out numerical simulations for three valve orientation angles. Because of

the axisymmetric inflow in our simulations, due to the fact that the flow through the valve is driven by a prescribed flow wave form and not a contracting ventricle, the valve orientation may not have as much of an effect in systole as in diastole. During diastole the anatomic aorta creates highly asymmetric secondary flow and complex flow patterns in the sinus region, which, as we will show in this work, make the valve closure dynamics a strong function of orientation. Therefore, the focus of this work is to quantify the effect of orientation during the diastolic phase and on the valve closure with emphasis on leaflet kinematics and the instantaneous hemodynamic environment. To the best of our knowledge, this is the first computational work to attempt a systematic investigation of the effect of BMHV orientation.

This paper is organized as follows. In Sec. 2 we briefly describe the numerical method and present the overall computational set-up and discuss various computational details. In Sec. 3 we report the results of the simulations in terms of the leaflet kinematics and flow physics in the anatomic aorta for different orientations. Finally, in Sec. 4 we discuss the key findings of this work.

2 Materials and Methods

2.1 The Numerical Method

The fluid-structure interaction solver we employ in this work has been extensively described and thoroughly validated against experimental data for a BMHV implanted in a straight axisymmetric aorta [32]. Furthermore, it has been successfully applied to simulate the flow in a BMHV implanted in an anatomically realistic aorta [33]. Therefore, only a brief description of the numerical method is presented in what follows. For more details about the method, the reader is referred to our previous publications [32,33].

The FSI solver adopts the partitioned approach, in which the FSI problem is partitioned into two separate fluid and structure domains [34]. The fluid and the structure domains are coupled through the boundary conditions at the interface of the two domains. The domains are loosely coupled if the boundary conditions at the interface are obtained from the domain solutions at the previous time level (explicit in time), while they are strongly coupled if the boundary conditions at the interface are obtained from the domain solutions at the current time level (implicit in time) [34]. Both loose and strong coupling FSI strategies (called LC-FSI and SC-FSI, respectively, hereafter) are implemented in our solver (see Ref. [32] for details). Numerical experiments and theoretical stability considerations presented in Ref. [32] suggest that under certain conditions, e.g., opening phase of the leaflets, unconditionally unstable FSI iterations result even when SC-FSI is employed. For such cases, however, combining SC-FSI with under-relaxation in conjunction with the Aitken acceleration technique was shown to effectively resolve the stability problems [32].

The motion of the leaflets is governed by the angular momentum equation around the hinge axis, which comprises a system of second-order ordinary differential equations [32,33]. These equations are solved numerically by first transforming them into a system of first-order ordinary differential equations and integrated in time using the trapezoidal rule [32,33].

The governing equations for the fluid (blood) domain are the three-dimensional, unsteady incompressible continuity and Navier-Stokes equations, which are solved in a domain containing multiple, 3D, arbitrarily complex moving immersed boundaries (leaflets) using the sharp-interface curvilinear-immersed boundary (CURVIB) solver of Ge and Sotiropoulos [35]. In the CURVIB approach, a curvilinear grid system is adopted to serve as the background grid and the immersed bodies are treated as sharp-interface immersed

boundaries. The sharp-interface immersed boundary method, enhanced with an efficient node classification algorithm described in Ref. [32], can easily handle large movements/deformations of multiple immersed bodies and is shown to be second-order accurate in space and time [36,37]. The curvilinear background mesh is adopted to enhance algorithmic flexibility and efficiency for internal flow problems in which the background domain, such as the anatomic aortic lumen in our case, can be efficiently discretized with a boundary-conforming curvilinear mesh. The equations are integrated in time using an efficient, second-order accurate fractional step methodology coupled with a Jacobian-free, Newton-Krylov solver for the momentum equations and a GMRES solver enhanced with multigrid as preconditioner for the Poisson equation. For more details about the flow solver, the readers are referred to Ref. [35].

2.2 Computational Details

The anatomic aorta geometry was provided to us by the Cardiovascular Fluid Mechanics Laboratory at the Georgia Institute of Technology and was reconstructed from the MRI of a healthy volunteer with a method similar to that presented by de Zelicourt et al. [38]. The main aortic branches on the aortic arch, i.e., the coronary arteries, the innominate artery, the left and right carotids, and the left subclavian artery, have been removed to simplify the outflow condition [33]. The computational domain is identical to that used by Borazjani et al. [33], namely, the inlet is a straight circular pipe 4D long while the outlet is also a straight pipe 2.25D long extended after the aortic arc with a cross section identical to the cross section at the end of the anatomic aorta (see Fig. 2(*a*)). The inlet is circular and has not been extended with a cross section of the anatomic aorta MRI inlet to avoid nonphysiologic inflow and achieve a symmetric inflow similar to the straight aorta simulations [33]. A body-fitted curvilinear grid with $201 \times 201 \times 253 \approx 10^7$ grid nodes has been used to discretize the empty aorta as in our previous work [33]. Based on the results of our previous validation studies [32,33], such high-resolution grid was found adequate to capture both the valve kinematics and the ensuing hemodynamics with good accuracy.

The valve and the housing geometry (clinical quality, St. Jude Regent, 23 mm valve) are discretized with a triangular mesh, as required by the CURVIB method (Fig. 1(*a*)). The valve is placed in three different orientations, each positioned 45 deg from the other, in the background of an anatomic aorta body-fitted mesh, at the end of the straight inlet section, and in the sinus area of the anatomic arc section, as shown in Fig. 2. The 0 deg orientation corresponds to the orientation in our previous work [33], in which the valve plane of symmetry (the one parallel to the two leaflets) is parallel to the ascending aorta's plane of curvature, as seen in Fig. 2(*a*); the ascending aorta (AA) is almost symmetric about its plane of curvature. Therefore, the 90 deg orientation is perpendicular to the aorta plane of curvature, while the 45 deg orientation is between the 0 deg and 90 deg orientations.

The reduced-inertia of the valve I_{red}=0.001 is similar to our previous work [33], which was calculated by assuming Polycarbonate as the leaflet material with the density of 1750 kg/m^3 and blood as fluid with the density of 1030 kg/m^3. As in our previous work [32,33], we have neglected the hinge mechanism connecting the leaflets and the valve housing. In addition, the damping due to the friction of the hinge has been neglected as well, since it is very small relative to the flow forces and moreover, no experimental data are available on the actual value of the friction coefficient. At the outflow, we use the convective boundary condition as in Refs. [32,33]. At the inflow, we prescribe unsteady, pulsatile plug flow based on the experimental data reported in Ref. [5]. Figure 3 shows the corresponding experimental time history of flow rate within a cardiac cycle with the peak flow rate of 24.27 l/min. Similar to our previous work [33], we have simulated one cardiac cycle, which according to the experiment [5] has the time period of 860 ms and the peak Reynolds number of 6000 based on the upstream pipe diameter (25.4 mm) and peak bulk velocity. The physical time step of

Δt=0.33 ms, corresponding to about 2580 time steps per cardiac cycle, is used in the all different orientation simulations identical to our previous works [32,33].

As we have extensively discussed in Ref. [32], obtaining converged FSI iterations for the BMHV problem is a particularly challenging task because of the combined effects of the leaflet properties (very low reduced inertia) and local flow effects. The low reduced inertia of the leaflets causes the motion of the leaflets to be dominated by the added-mass effect, which in general has a detrimental effect on the stability of FSI iterations. Nevertheless, as in our previous work [33], the under-relaxed SC-FSI combined with the Aitken acceleration technique [32] could reduce the residual (i.e., the difference in the angular velocity and position of each leaflet between two successive iterations) by about four orders of magnitude to 10^{-6} within four to five SC-FSI iterations. Furthermore, at each time instant as the pulsatile inflow flow rate changed, the Poisson solver (GMRES with multigrid as preconditioner) conserves mass discretely at each grid cell by driving the discrete divergence of the velocity to machine zero within 30 GMRES iterations. The simulations provide the leaflet kinematics and the 3D flow field for each orientation of BMHV implantation.

3 Results

In this section, we present the results of our numerical simulations for the three BMHV implantation orientations. We first present the calculated leaflet kinematics for each case. Subsequently, we visualize and discuss the ensuing hemodynamics and finally focus on quantifying the viscous shear stress environment for each case.

3.1 Leaflet Kinematics

The calculated leaflet kinematics for different orientations are plotted in Fig. 3. It can be observed in this figure that all orientations open quite similarly. As we have already discussed before, this finding is not surprising since there is no contracting ventricle in our model and instead, the systolic flow is driven by the axisymmetric plug inflow waveform. It is evident from Fig. 3, however, that striking differences are present in the closing kinematics among the three cases. For all orientations, one leaflet starts closing earlier than the other (for convenience, we shall refer to the first-to-close leaflet as leaflet 1). Comparing the motion of leaflet 1 for the different orientations, it can be observed that for the 90 deg orientation, leaflet 1 starts to close earlier than the 45 deg orientation case, while for the 45 deg case, leaflet 1 starts to close earlier than in the 0 deg orientation. The reverse is true for the other leaflet (referred to as leaflet 2), i.e., the 0 deg orientation closing is followed by that in 45 deg and 90 deg orientations, respectively. Turning now our attention to the degree of asymmetry of the kinematics of the two leaflets, we observed from Fig. 3 that the 0 deg orientation leaflets close almost symmetrically. In fact, for this case, leaflet 1 closes only 1 ms later than leaflet 2. The asymmetry in the closing of the leaflets, however, greatly increases with increasing the orientation angle. Namely, leaflet 2 closes 41 ms and 76 ms after leaflet 1 in 45 deg and 90 deg orientations, respectively. The rebound of leaflet 1 after closing also increases with increase in orientations, i.e., the 0 deg orientation has the smallest rebound while the 90 deg orientation shows the largest rebound. An interesting feature observed during the closing is that leaflet 2 in the 90 deg and 45 deg orientations rebound at the start of closing, i.e., they start to close but open fully again before starting to finally close. The importance of valve rebound and closure asymmetry will be discussed extensively in Sec. 4.

3.2 Instantaneous Hemodynamics

The previously discussed differences in the leaflet kinematics during the closing phase correspond to differences in ensuing hemodynamics for each valve orientation. To visualize and compare the underlying hemodynamics for each case, we plot in Fig. 4 the contours of out-of-plane vorticity in the respective midplane of the valve for each orientation at various time instants identified in Fig. 3. Note that it is important to keep in mind, as we discuss and interpret the results reported in this section, that the visualization plane passes through different parts of the aorta geometry for each orientation. Qualitatively, we see similar vortex dynamics for all three orientations in early systole (Fig. 4(*a*)), characterized by organized vortical structures shed from the leaflets and the sinus as observed in the experiments [5] and our previous simulations [32,33]. Near the peak systole (Fig. 4(*b*)), the organized shear layers break down rapidly into small-scale vortical structures. After the peak systole, the flow is dominated by wormlike turbulent structures, which persist even after the peak diastole (Figs. 4(*c*) and 4(*d*)). In general, the near wake of the leaflets is quite similar for all three cases during the opening phase (Fig. 4(*a*)) but significant differences are observed as a function of orientation in the closing phase (Fig. 4(*d*)), which is consistent with the previously discussed differences in leaflet kinematics.

The three-dimensional vortical structures are visualized in Fig. 5 using the q-criterion [39] at different time instants within the cardiac cycle for the three different valve orientations. It can be observed that for all orientations, similar to what was discussed before in terms of vorticity and previously observed experimental and computational results [5,32], the vortical structures are well organized and laminar in the early systole (Fig. 5(*a*)) but break down in an explosive manner into small-scale chaotic vortical structures just before the peak systole (Fig. 5(*b*)). In the early systole (Fig. 5(*a*)) the 0 deg and 90 deg orientations develop a sinus ring with an azimuthal mode-3 modulation, which follows the shape of the triple-cusp sinus. However, in the 45 deg orientation, the modulation of the sinus ring in the right coronary artery (RCA) cusp is not fully developed, which results in a V-shaped ring developing mainly in the NCC and the left coronary artery (LCA). Nevertheless, the vortical structures due to shedding from the leaflets are quite similar and not dependent on the orientating of the leaflet (Fig. 5(*a*)). The chaotic turbulent-like state (Figs. 5(*c*) and 5(*d*)), which persists throughout the rest of the cardiac cycle after peak systole, is highly asymmetric. Consequently, the valve orientation should affect the interaction of the leaflets with such asymmetric flow field. Given the above documented differences in the vorticity dynamics for each orientation during closing, it is reasonable to also anticipate differences in the respective pressure fields. Figure 6 shows the pressure on the midplane of the valve for each orientation at peak diastole-instant (d) in Fig. 3. For the 0 deg orientation in which the leaflets close nearly symmetrically, the pressure field exhibits, as one would expect, less asymmetry relative to the other orientations. This is probably due to the fact that in this orientation, the valve is orientated such that the ascending aorta curvature plane nearly coincides with the valve plane of symmetry (see Fig. 2(*a*)) for the definition of the ascending aorta symmetry plane. For the 45 deg and 90 deg orientations, however, the pressure on the outer bend of the aorta is higher relative to the inner bend. For these orientations, the leaflets make an angle with the symmetry plane of the ascending aorta, i.e., one leaflet is closer to the outer bend and the other one is closer to the inner bend of the ascending aorta. Consequently, the direction of the curvature-induced pressure gradient that is set up to balance the centrifugal force is broadly aligned with the valve plane of symmetry that cuts through the two leaflets, giving rise to the large asymmetry in the resulting pressure fields. The leaflet near the outer bend always closes earlier since it experiences higher pressure on its aortic side as observed in Fig. 6.

3.3 Viscous Shear Stress

To evaluate the different flowfields in terms of the forces acting on blood cells, the instantaneous viscous stresses can be used to provide a measure of mechanical loads [31]. Since viscous stresses comprise a second-order tensor, a coordinate-independent metric is needed to quantify mechanical loads. Similar to Grigioni et al. [40], Travis et al. [24], and Ge et al. [31], the concept of local maximum stress is used herein as follows. The principal stresses of a given stress tensor τ_{ij} are the solutions of the following equation:

$$\sigma^3 - I_1\sigma^2 + I_2\sigma - I_3 = 0 \tag{1}$$

where I_1, I_2, and I_3 are the first, second, and third invariants of the tensor (repeated indices imply summation):

$$I_1 = \tau_{jj} \tag{2}$$

$$I_2 = \tau_{ij}\tau_{ij} \tag{3}$$

$$I_3 = \tau_{ij}\tau_{jk}\tau_{ki} \tag{4}$$

The coordinate invariant local maximum stress τ_{loc} is given by

$$\tau_{loc} = \frac{1}{2}(\sigma_{max} - \sigma_{min}) \tag{5}$$

where σ_{max} and σ_{min} are the maximum and minimum principal stresses.

As in our previous work [33], we calculate histograms of the local maximum shear stress values at a given instant in time to illustrate the distribution of τ_{loc} throughout the domain at that instant. The histograms plot the number of occurrence of τ_{loc} values in intervals of $\Delta\tau_{loc}$ = 0.064 Pa, normalized by the total number of occurrences and multiplied by 100 to be stated as percentile. Therefore, histograms can be viewed as the percentile of the aortic lumen volume that has a given value of τ_{loc}.

In Fig. 7, we plot the histogram of τ_{loc} for different valve orientations at different time instants within one cardiac cycle. We observe that the orientation does not significantly affect the distribution of local viscous shear in the aortic lumen. For all orientations, the histograms plotted in Fig. 7 decays exponentially with τ_{loc} at each time instant, i.e., most of the domain experiences low τ_{loc} and the high values occur less frequently in the domain. Furthermore, the histogram values correlate with the flow rate for high τ_{loc}, i.e., higher instantaneous values of flow rate correspond to larger areas of higher τ_{loc}. This trend is clearly shown in the inset of Fig. 7, which zooms into the large τ_{loc} values. It can be observed that the higher histogram values occur at peak systole (t_b), while the lowest values occur at peak diastole (t_d). To illustrate where the high values of τ_{loc} generally occur, we plot in Fig. 8 the isosurfaces of the local maximum shear stress τ_{loc} = 6.4 Pa for several time instants during the cardiac cycle. We observe that for all orientations, the high values of τ_{loc} occur near the valve region, as well as the aortic arch region, due to the curvature-induced secondary motion. The levels of τ_{loc}, in agreement with our histogram results, correlate very

well with the flow rate. In all orientations, as the flow rate increases toward the peak systole (see Figs. 8(*a*) and 8(*b*)), larger regions of high τ_{loc} are observed. After peak systole, when the flow rate decreases, the regions of higher τ_{loc} decrease in size as well (see Fig. 8(*b*)–8(*d*)). Again, in agreement with the histogram results (see the inset of Fig. 7), it can be observed that the flow in Fig. 8(*b*) has smaller regions of high τ_{loc} relative to Fig. 8(*c*), which has similar flow rate. This is due to the fact that in time instant (Fig. 8(*b*)), the flow is well organized with less structures in the aortic arch region but in Fig. 8(*c*), the flow has broken down into small vortical structures. Finally, we observe in Fig. 8 that the orientation does not significantly affect the regions of high shear stress.

4 Discussion

Intermittent regurgitation [41] is a well known problem of mechanical heart valves, which can be caused by the asymmetric closing of the leaflets and their rebound, allowing blood to leak backward to the left ventricle. This means that the left ventricle must pump more blood than normal and will gradually get bigger because of the extra workload. In a recent in vitro study, Enchinger et al. [42] showed that intermittent regurgitation could occur in an aortic ADVANTAGE valve in the horizontal orientation, in which gravity maximized the asymmetric closure of the leaflets. The asymmetric closure of the leaflets caused the leading edge of the second-to-close leaflet to make contact with the chamfer on the leading edge of the first-to-close leaflet [42]. In addition, the rebound of leaflets has been related to the formation of cavitation that might cause hemolysis and wear for tilting-disk MHVs [6]. Based on our results, we observed that the 90 deg orientation has the highest asymmetry and rebound between all the tested orientations, while the 0 deg orientation has the lowest. Consequently, we hypothesize that if the valve is implanted in the orientation symmetric relative to the symmetry plane of the ascending aorta curvature, it should be less susceptible to intermittent regurgitation and leaflet rebound. Of course, this hypothesis should be tested with more patient-specific simulations, in vitro and in vivo experiments. Furthermore, Enchinger et al. [42] reported a clinical case that an ADVANTAGE valve was replaced by another ADVANTAGE valve that also showed intermittent regurgitation. Therefore, they concluded that patient-specific factors—e.g., individual aortic geometry (the angle between the left ventricular outflow tract and ascending aorta, width of the ascending aorta, and sinuses of Valsalva), flow and pressure conditions, heart rhythm, aorta compliance, etc.—may contribute to intermittent regurgitation [42]. We have shown that the implantation orientation of the valve, as well as aorta geometry, affects the valve performance and hemodynamics. Therefore, performing a virtual surgery to optimize the placement of a mechanical valve before the surgery for patients based on the anatomical imaging data could be quite beneficial.

With regard to the effect of orientation on shear stress, we found no significant effects on the size of regions of high-shear stress as evident from the histograms at different time instants during the cycle. This is in agreement with the earlier work of Kleine et al. [25] who reported that the Reynolds stresses downstream of bileaflet valves (similar to the one used in our simulations) were less susceptible to orientation. It should be noted, however, that they measure Reynolds stresses as a metric of shear stress and valve hemodynamic performance while we calculate viscous shear stresses-see Ref [31] for a discussion on the Reynods versus viscous stress. This important difference not withstanding the findings of Kleine et al. considered together with our findings does point to the conclusion that valve orientation does not have a significant effect on the hemodynamic stresses experienced by blood elements.

Finally, we should mention that we have assumed the blood to be a Newtonian fluid. This assumption is reasonable for larger arteries such as the aorta. However, in cases, where the

size of the flow domain is in the same order of magnitude as the blood cell size (i.e., small arteries), the non-Newtonian effects should be taken into account. Other parameters such as compliance of the aortic walls and upstream/downstream boundary conditions can affect the simulations, as well. The blood flow distribution between different arteries that branch from the aorta is also important in determining the downstream boundary conditions, as shown in Ref. [43]. Furthermore, due to the simplified inflow of our simulations, we focused our attention on the diastolic (closure) performance of the BMHVs in this study. The angle between the valve axis and the left ventricle axis has been hypothesized to affect the systolic performance of the valves [26]. In order to assess the systolic performance, we need to model the aortic valve in the left-heart system with a realistic left ventricle motion. The work on creating a physiological left-heart system to assess the performance of a BMHV is in progress and will be reported in future communications.

Acknowledgments

This work was supported by the NIH Grant No. RO1–HL-07262 and the Minnesota Supercomputing Institute. We thank Ajit Yoganathan and the members of the Cardiovascular Fluid Mechanics Laboratory for providing us with the anatomic aorta geometry used in this study.

References

1. Anderson GH, Hellums JD, Moake J, Al-frey CP Jr. Platelet Response to Shear Stress: Changes in Serotonin Uptake, Serotonin Release, and ADP Induced Aggregation. Thromb. Res. 1978; 13(6): 1039–1047. [PubMed: 749261]
2. Holme PA, Orvim U, Hamers M, Solum NO, Brosstad FR, Barstad RM, Sakariassen KS. Shear-Induced Platelet Activation and Platelet Microparticle Formation at Blood Flow Conditions as in Arteries With a Severe Stenosis. Arterioscler., Thromb., Vasc. Biol. 1997; 17(4):646–653. [PubMed: 9108776]
3. Schoephoerster RT, Oynes F, Nunez G, Kapadvan-jwala M, Dew-anjee MK. Effects of Local Geometry and Fluid Dynamics on Regional Platelet Deposition on Artificial Surfaces. Arterioscler., Thromb., Vasc. Biol. 1993; 13(12):1806–1813.
4. Stein PD, Sabbah HN. Measured Turbulence and Its Effect on Thrombus Formation. Circ. Res. 1974; 35(4):608–614. [PubMed: 4278187]
5. Dasi LP, Ge L, Simon HA, Sotiropoulos F, Yoganathan AP. Vorticity Dynamics of a Bileaflet Mechanical Heart Valve in an Axisymmetric Aorta. Phys. Fluids. 2007; 19:067105.
6. Kini V, Bachmann C, Fontaine A, Deutsch S, Tarbell J. Flow Visualization in Mechanical Heart Valves: Occluder Rebound and Cavitation Potential. Ann. Biomed. Eng. 2000; 28(4):431–441. [PubMed: 10870900]
7. Ellis JT, Healy TM, Fontaine AA, Saxena R, Yoganathan AP. Velocity Measurements and Flow Patterns Within the Hinge Region of a Medtronic Parallel Bileaflet Mechanical Valve With Clear Housing. J. Heart Valve Dis. 1996; 5(6):591–599. [PubMed: 8953436]
8. Liu JS, Lu PC, Chu SH. Turbulence Characteristics Downstream of Bileaflet Aortic Valve Prostheses. ASME J. Biomech. Eng. 2000; 122(2):118–124.
9. Manning KB, Kini V, Fontaine AA, Deutsch S, Tarbell JM. Regurgitant Flow Field Characteristics of the St. Jude Bileaflet Mechanical Heart Valve Under Physiologic Pulsatile Flow Using Particle Image Velocimetry. Artif. Organs. 2003; 27(9):840–846. [PubMed: 12940907]
10. Nyboe C, Funder JA, Smerup MH, Nygaard H, Hasenkam JM. Turbulent Stress Measurements Downstream of Three Bileaflet Heart Valve Designs in Pigs. Eur. J. Cardiothorac. Surg. 2006; 29(6):1008–1013. [PubMed: 16675253]
11. Nygaard H, Paulsen PK, Hasenkam JM, Pedersen EM, Rovsing PE. Turbulent Stresses Downstream of Three Mechanical Aortic Valve Prostheses in Human Beings. J. Thorac. Cardiovsc. Surg. 1994; 107:438–446.
12. Yoganathan AP, Woo YR, Sung HW. Turbulent Shear Stress Measurements in the Vicinity of Aortic Heart Valve Prostheses. J. Biomech. 1986; 19(6):433–442. [PubMed: 2943742]

13. Bluestein D, Li Y, Krukenkamp I. Free Emboli Formation in the Wake of Bi-Leaflet Mechanical Heart Valves and the Effects of Implantation Techniques. J. Biomech. 2002; 35(12):1533–1540. [PubMed: 12445606]
14. Bluestein D, Rambod E, Gharib M. Vortex Shedding as a Mechanism for Free Emboli Formation in Mechanical Heart Valves. ASME J. Biomech. Eng. 2000; 122((2)):125–134.
15. Cheng R, Lai YG, Chandran KB. Three-Dimensional Fluid-Structure Interaction Simulation of Bileaflet Mechanical Heart Valve Flow Dynamics. Ann. Biomed. Eng. 2004; 32(11):1471–1483. [PubMed: 15636108]
16. De Hart J, Peters G, Schreurs P, Baaijens F. A Three-Dimensional Computational Analysis of Fluid-Structure Interaction in the Aortic Valve. J. Biomech. 2003; 36(1):103–112. [PubMed: 12485644]
17. Grigioni M, Daniele C, Del Gaudio C, Morbiducci U, Balducci A, D'Avenio G, Barbaro V. Three-Dimensional Numeric Simulation of Flow Through an Aortic Bileaflet Valve in a Realistic Model of Aortic Root. ASAIO J. 2005; 51(3):176–183. [PubMed: 15968945]
18. Krishnan S, Udaykumar H, Marshall J, Chan-dran K. Two-Dimensional Dynamic Simulation of Platelet Activation During Mechanical Heart Valve Closure. Ann. Biomed. Eng. 2006; 34(10): 1519–1534. [PubMed: 17013660]
19. Nobili M, Morbiducci U, Ponzini R, Del Gaudio C, Balducci A, Grigioni M, Maria Montevecchi F, Redaelli A. Numerical Simulation of the Dynamics of a Bileaflet Prosthetic Heart Valve Using a Fluid-Structure Interaction Approach. J. Biomech. 2008; 41(11):2539–2550. [PubMed: 18579146]
20. Pedrizzetti G, Domenichini F. Asymmetric Opening of a Simple Bileaflet Valve. Phys. Rev. Lett. 2007; 98(21):214503. [PubMed: 17677780]
21. Tai C, Liew K, Zhao Y. Numerical Simulation of 3D Fluid-Structure Interaction Flow Using an Immersed Object Method With Overlapping Grids. Comput. Struct. 2007; 85(11–14):749–762.
22. Sotiropoulos F, Borazjani I. A Review of State-Of-The-Art Numerical Methods for Simulating Flow Through Mechanical Heart Valves. Med. Biol. Eng. Comput. 2009; 47(3):245–256. [PubMed: 19194734]
23. Yoganathan AP, He Z, Jones SC. Fluid Mechanics of Heart Valves. Annu. Rev. Biomed. Eng. 2004; 6:331–362. [PubMed: 15255773]
24. Travis BR, Leo HL, Shah PA, Frakes DH, Yoganathan AP. An Analysis of Turbulent Shear Stresses in Leakage Flow Through a Bileaflet Mechanical Prostheses. ASME J. Biomech. Eng. 2002; 124(2):155–165.
25. Kleine P, Perthel M, Nygaard H, Hansen SB, Paulsen PK, Riis C, Laas J. Medtronic Hall Versus St. Jude Medical Mechanical Aortic Valve: Downstream Turbulences With Respect to Rotation in Pigs. J. Heart Valve Dis. 1998; 7(5):548–555. [PubMed: 9793855]
26. Laas J, Kleine P, Hasenkam M, Nygaard H. Orientation of Tilting Disc and Bileaflet Aortic Valve Substitutes for Optimal Hemodynamics. Ann. Thorac. Surg. 1999; 68(3):1096–1099. [PubMed: 10510028]
27. Kleine P, Perthel M, Hasenkam J, Nygaard H, Hansen S, Laas J. High Intensity Transient Signals (HITS) as a Parameter for Optimum Orientation of Mechanical Aortic Valves. Thorac. Cardiovasc. Surg. 2000; 48(6):360–363. [PubMed: 11145405]
28. Kleine P, Perthel M, Hasenkam J, Nygaard H, Hansen S, Laas J. Downstream Turbulence and High Intensity Transient Signals (HITS) Following Aortic Valve Replacement With Medtronic Hall or St. Jude Medical Valve Substitutes. Eur. J. Cardiothorac. Surg. 2000; 17(1):20–24. [PubMed: 10735407]
29. Kleine P, Scherer M, Abdel-Rahman U, Klesius A, Ackermann H, Moritz A. Effect of Mechanical Aortic Valve Orientation on Coronary Artery Flow: Comparison of Tilting Disc Versus Bileaflet Pros-Theses in Pigs. J. Thorac. Cardiovasc. Surg. 2002; 124(5):925–932. [PubMed: 12407375]
30. van't Veer M, van Straten B, vande Vosse F, Pijls N. Influence of Orientation of Bi-Leaflet Valve Prostheses on Coronary Perfusion Pressure in Humans. Interact. Cardiovasc. Thorac. Surg. 2007; 6(5):588–592. [PubMed: 17670729]
31. Ge L, Dasi LP, Sotiropoulos F, Yoganathan AP. Characterization of Hemodynamic Forces Induced by Mechanical Heart Valves: Reynolds vs. Viscous Stresses. Ann. Biomed. Eng. 2008; 36(2):276–297. [PubMed: 18049902]

32. Borazjani I, Ge L, Sotiropoulos F. Curvilinear Immersed Boundary Method for Simulating Fluid Structure Interaction With Complex 3D Rigid Bodies. J. Comput. Phys. 2008; 227(16):7587–7620. [PubMed: 20981246]
33. Borazjani I, Ge L, Sotiropoulos F. High-Resolution Fluid-Structure Interaction Simulations of Flow Through a Bi-Leaflet Mechanical Heart Valve in an Anatomic Aorta. Ann. Biomed. Eng. 2010; 38(2):326–344. [PubMed: 19806458]
34. Borazjani, I. Ph.D. thesis. Twin Cities, Minnesota, USA: University of Minnesota; 2008. Numerical Simulations of Fluid/Structure Interaction Problems in Biological Flows.
35. Ge L, Sotiropoulos F. A Numerical Method for Solving the 3D Unsteady Incompressible Navier Stokes Equations in Curvilinear Domains With Complex Immersed Boundaries. J. Comput. Phys. 2007; 225(2):1782–1809. [PubMed: 19194533]
36. Borazjani I, Sotiropoulos F. Numerical Investigation of the Hydrodynamics of Carangiform Swimming in the Transitional and Inertial Flow Regimes. J. Exp. Biol. 2008; 211:1541–1558. [PubMed: 18456881]
37. Gilmanov A, Sotiropoulos F. A Hybrid Cartesian/Immersed Boundary Method for Simulating Flows With 3D, Geometrically Complex, Moving Bodies. J. Comput. Phys. 2005; 207(2):457–492.
38. de Zélicourt D, Pekkan K, Kitajima H, Frakes D, Yoganathan A. Single-Step Stereolithography of Complex Anatomical Models for Optical Flow Measurements. ASME J. Biomech. Eng. 2005; 127:204–207.
39. Hunt J, Wray A, Moin P. Eddies, Streams, and Convergence Zones in Turbulent Flows. Studying Turbulence Using Numerical Simulation Databases, 2: Proceedings of the 1988 Summer Program. 1988:193–208. Paper No. SEE N89-2453818-34.
40. Grigioni M, Daniele C, D'Avenio G, Barbaro V. Evaluation of the Surface-Averaged Load Exerted on a Blood Element by the Reynolds Shear Stress Field Provided by Artificial Cardiovascular Devices. J. Biomech. 2002; 35(12):1613–1622. [PubMed: 12445614]
41. Allen P, Robertson R. The Significance of Intermittent Regurgitation in Aortic Valve Prostheses. J. Thorac. Cardiovasc. Surg. 1967; 54(4):549–556. [PubMed: 6051442]
42. Eichinger W, Hettich I, Bleiziffer S, Günzinger R, Hutter A, Bauern-schmitt R, Lange R. Intermittent Regurgitation Caused by Incomplete Leaflet Closure of the Medtronic ADVANTAGE Bileaflet Heart Valve: Analysis of the Underlying Mechanism. J. Thorac. Cardiovas. Surg. 2010; 140(3):611–616.
43. Grinberg L, Karniadakis G. Outflow Boundary Conditions for Arterial Networks With Multiple Outlets. Ann. Biomed. Eng. 2008; 36(9):1496–1514. [PubMed: 18612828]

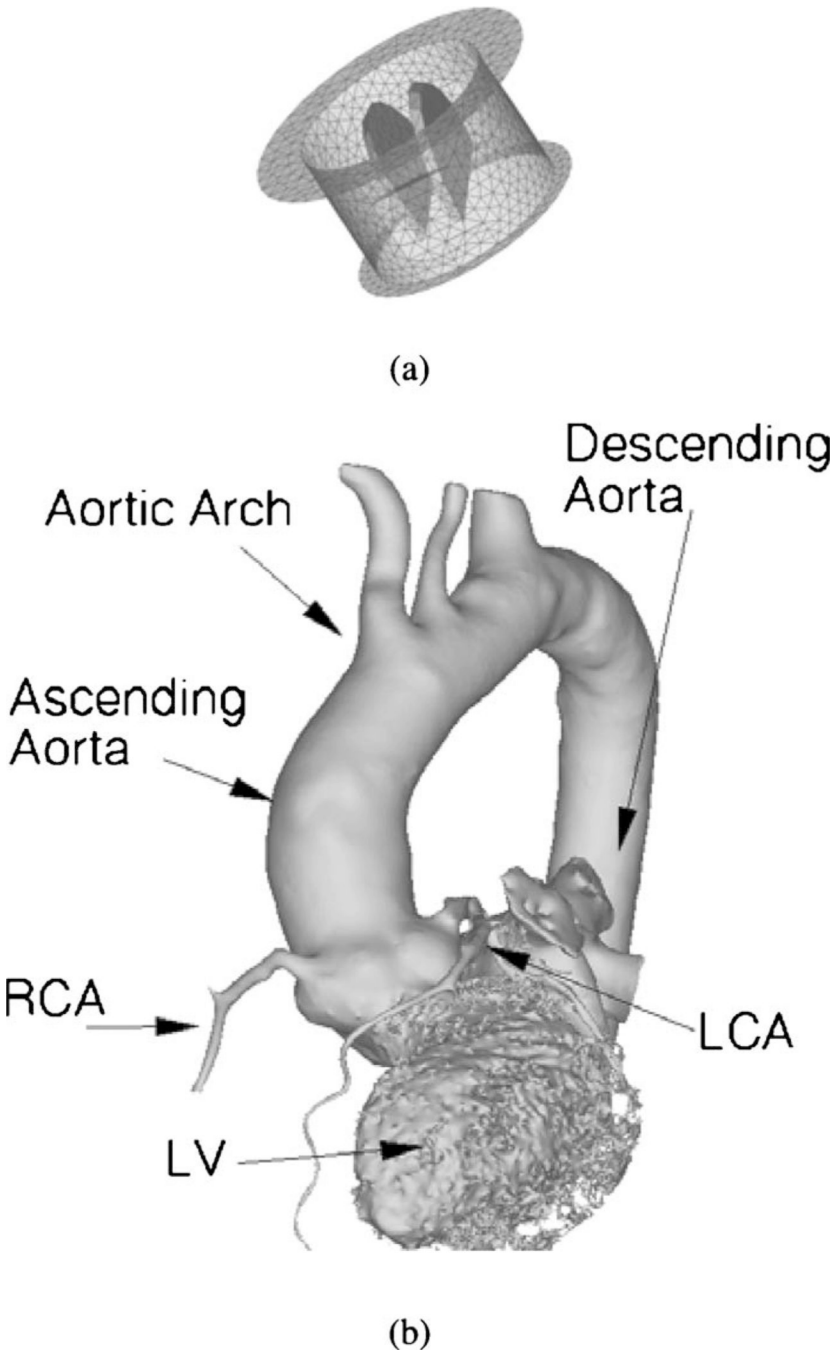

Fig. 1.

(*a*) A typical bileaflet mechanical heart valve meshed with triangular elements, as required by the CURVIB method. (*b*) The anatomy of the left side of the heart. The ascending aorta has a curvature different from that of the aortic arch; LV: left ventricle; NCA: noncoronary artery; RCA: right coronary artery; LCA: left coronary artery.

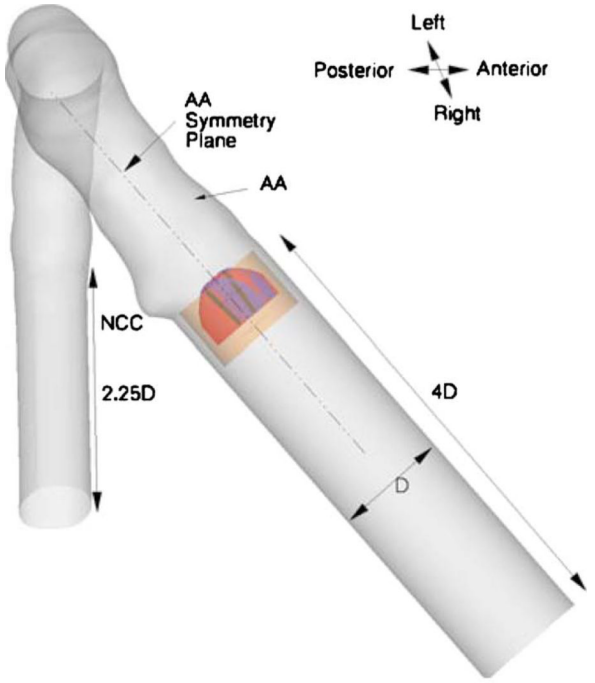

(a)

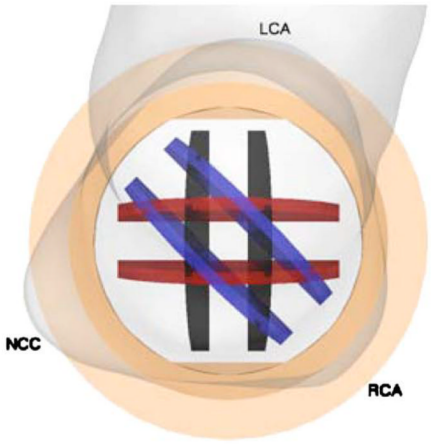

(b)

Fig. 2.

(*a*) The anatomically realistic aorta geometry reconstructed from MRI data with the straight inlet and outlet additions as in Ref. [33] and the placement of the valves at different orientations inside it. The ascending aorta is almost symmetric about its plane of curvature (dash-double-dot line). (*b*) The placement of the valves inside the sinus from top view. The original orientation of the leaflet (vertical leaflets) [33] was parallel to the plane of curvature of the ascending aorta. The 90 deg orientation (horizontal leaflets) are perpendicular to this plane of curvature while the 45 deg orientation (inclined leaflets) is in between.

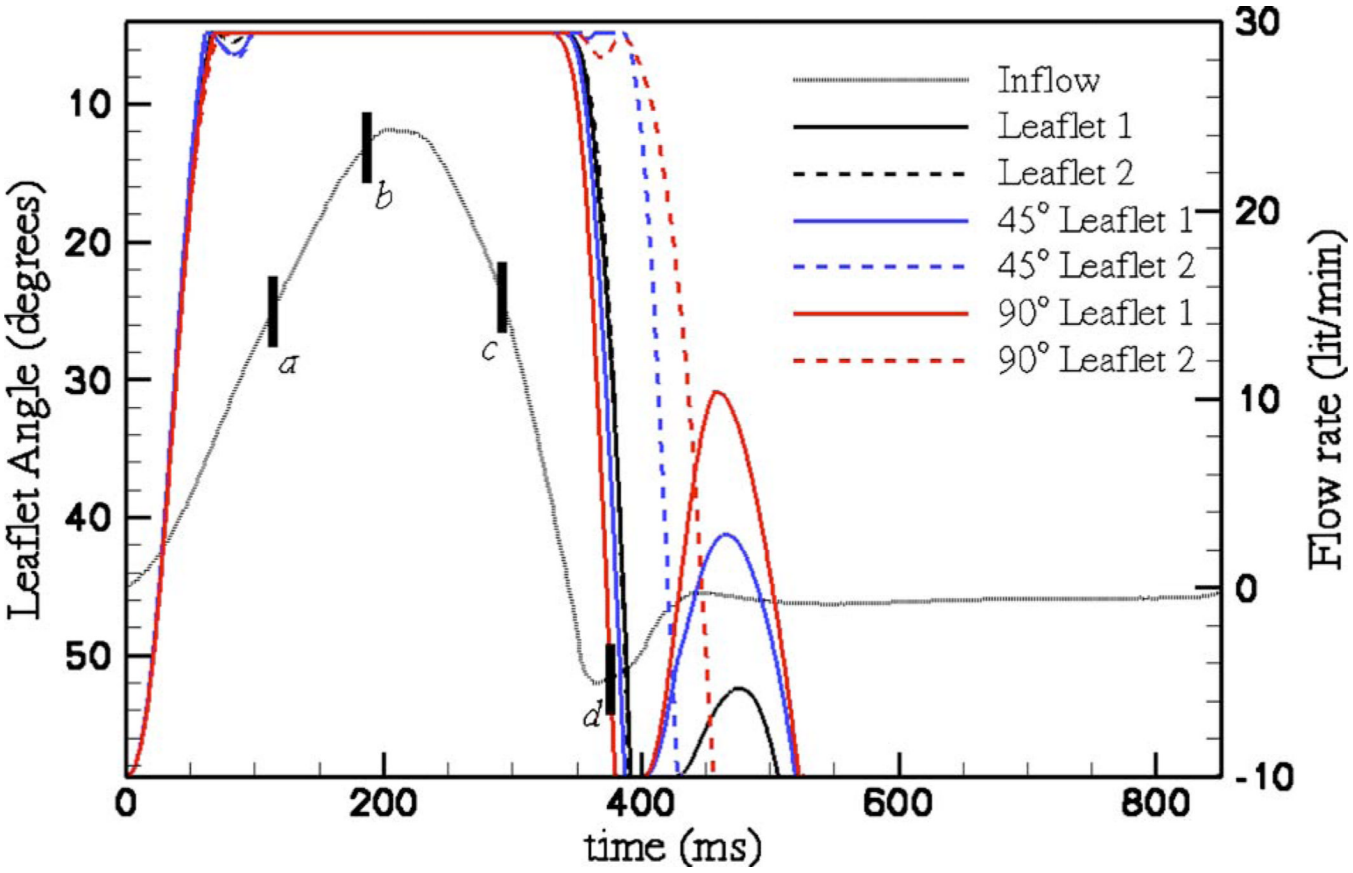

Fig. 3.

Physiological incoming flow waveform specified at the inlet and the leaflet kinematics for the BMHV in an anatomic aorta at different orientations. The time instants in the cardiac cycle in which the flow is visualized are marked with thick vertical lines *a*, *b*, *c*, and *d*.

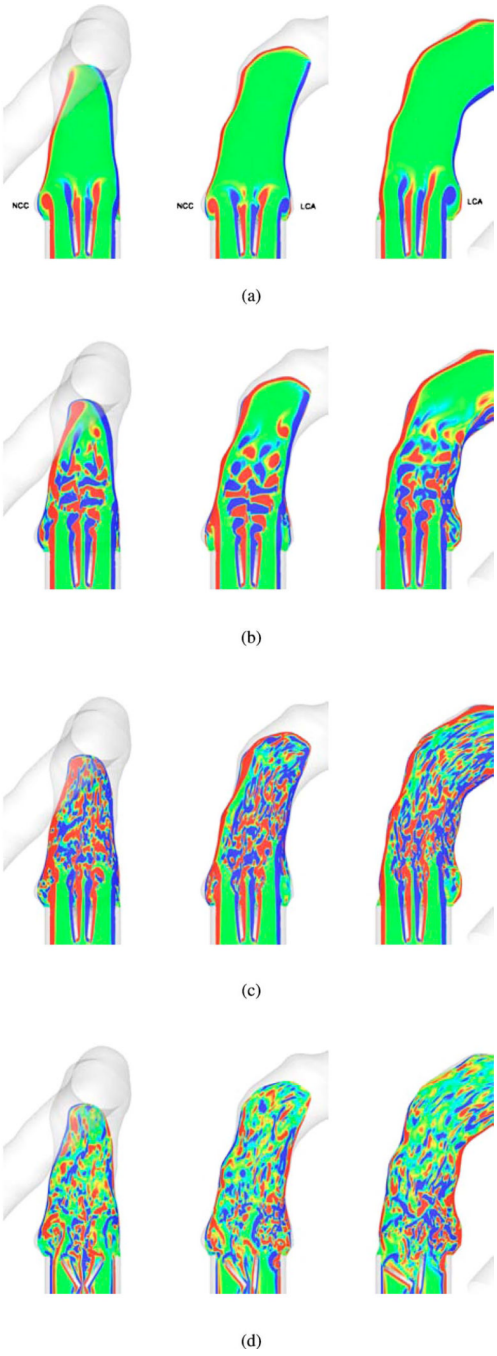

Fig. 4.

Comparison of instantaneous out-of-plane nondimen-sional vorticity ($\Omega D/U$) contours for 0 deg (left), 45 deg (middle), and 90 deg (right) orientations on the midplane of the valve. *a*, *b*, *c*, etc., correspond to the time instant marked in Fig. 3 within the cardiac cycle.

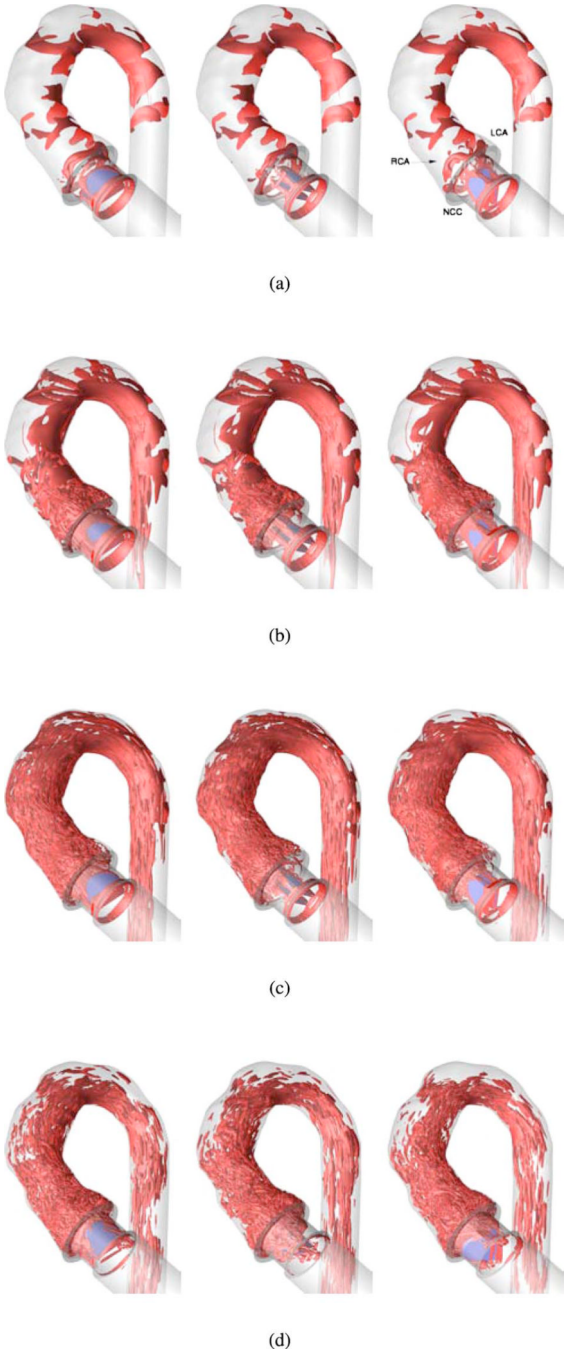

Fig. 5.

Comparison of vortical structures visualized by the iso-surface of q-criteria for 0 deg (left), 45 deg (middle), and 90 deg (right) orientations. *a*, *b*, *c*, etc., correspond to the time instant marked in Fig. 3 within the cardiac cycle.

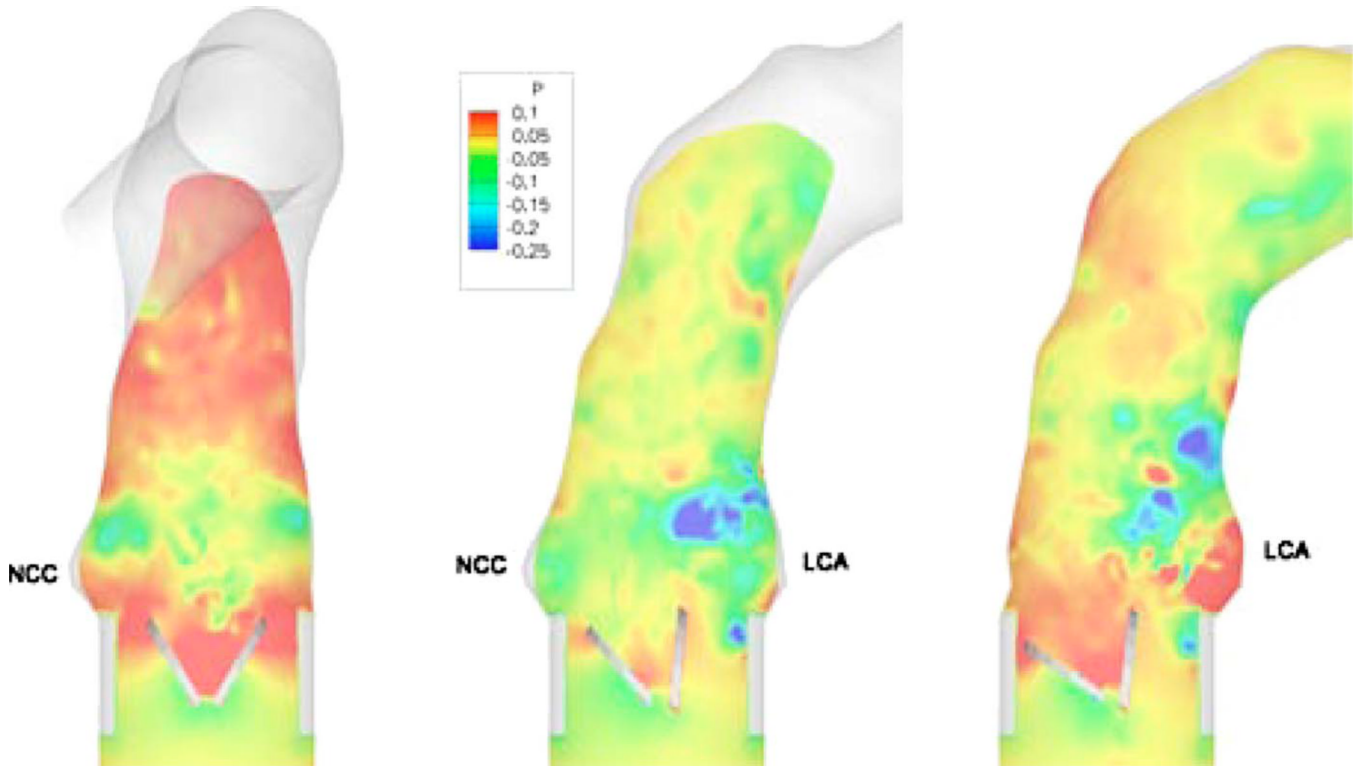

Fig. 6.

Instantaneous nondimensional pressure ($p/\rho U^2$) contours for 0 deg (left), 45 deg (middle), and 90 deg (right) orientations on the midplane of the valve corresponding to the time instant *d* marked in Fig. 3.

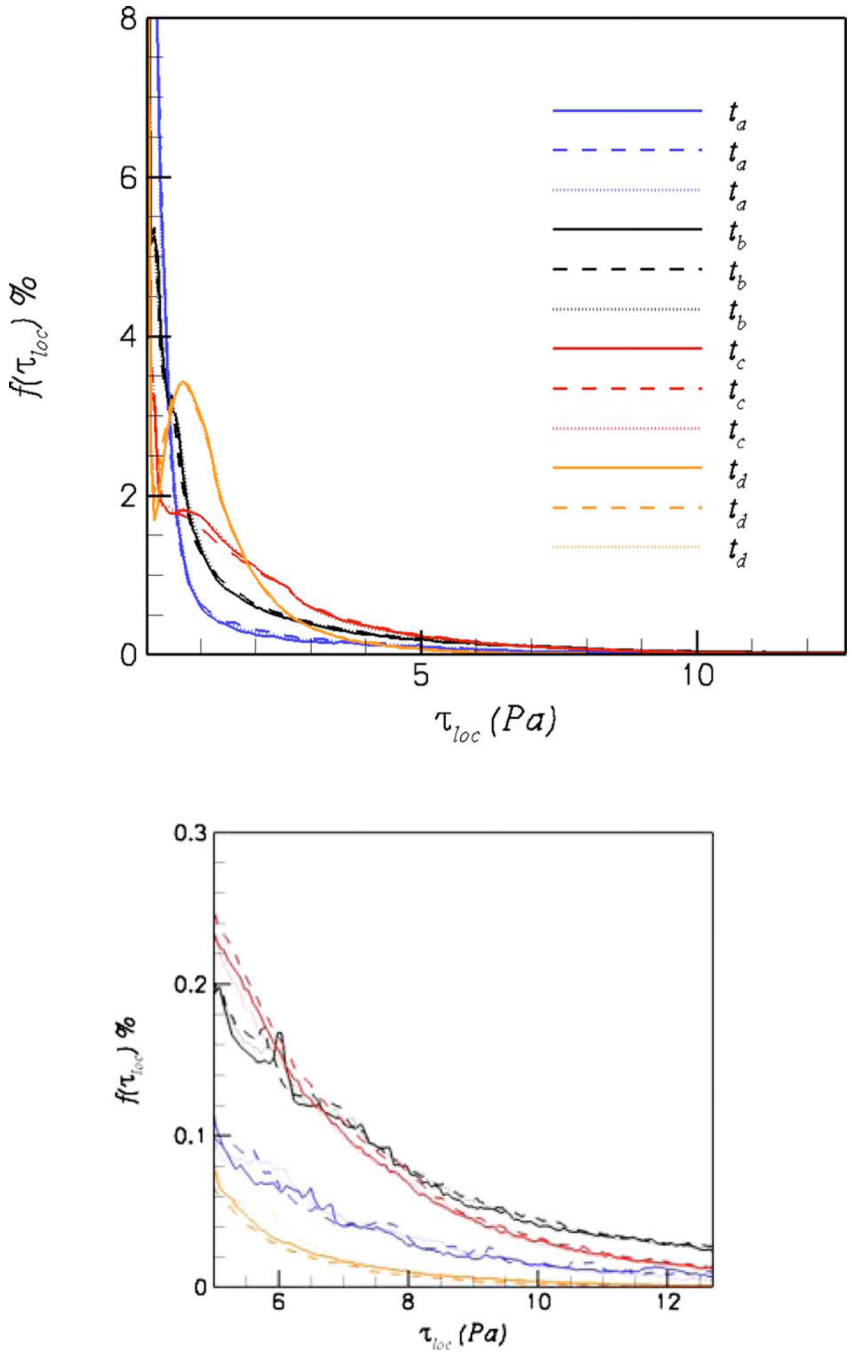

Fig. 7.

Histograms of local maximum shear τ_{loc} in the anatomic aorta for 0 deg (dotted lines), 45 deg (solid lines), and 90 deg (dashed lines) orientations. *f* is the percentile of the number of occurrences of a shear value τ_{loc} values in intervals with the width $\Delta\tau_{loc}$=0.064 Pa to the total number of occurrences. *a*, *b*, *c*, etc., correspond to the time instant marked in Fig. 3 within the cardiac cycle.

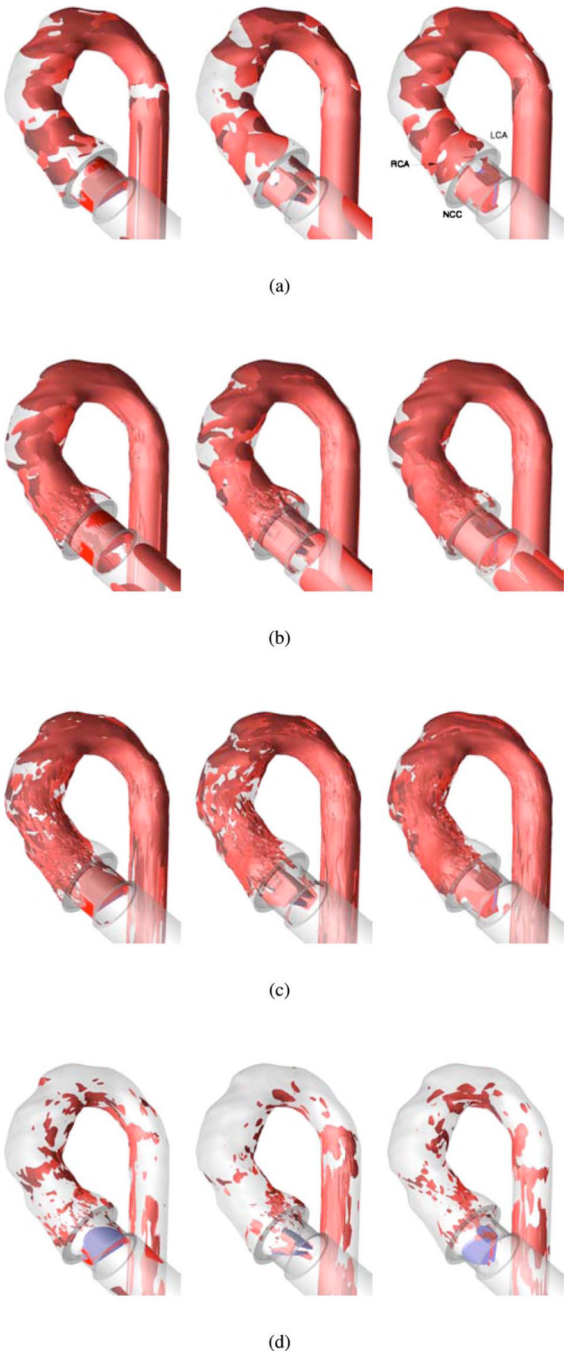

Fig. 8.

Comparison of instantaneous isosurfaces of local maximum shear τ_{loc}=6.4 Pa for 0 deg (left), 45 deg (middle), and 90 deg (right) orientations. *a*, *b*, *c*, etc., correspond to the time instant marked in Fig. 3 within the cardiac cycle.